Liquid Crystals
Publication details, including instructions for authors and subscription information:
http://www.informaworld.com/smpp/title~content=t713926090

Phase transitions in ferroelectric liquid crystals in a restricted geometry

T. Povše[a]; I. Muševič[a]; B. Žekš[a]; R. Blinc[a]
[a] Stefan Institute, University of Ljubljana, Ljubljana, Slovenia

To cite this Article Povše, T. , Muševič, I. , Žekš, B. and Blinc, R.(1993) 'Phase transitions in ferroelectric liquid crystals in a restricted geometry', Liquid Crystals, 14: 5, 1587 — 1598
To link to this Article: DOI: 10.1080/02678299308026470
URL: http://dx.doi.org/10.1080/02678299308026470

LIQUID CRYSTALS, 1993, VOL. 14, NO. 5, 1587–1598

Phase transitions in ferroelectric liquid crystals in a restricted geometry

by T. POVŠE, I. MUŠEVIČ, B. ŽEKŠ and R. BLINC
J. Stefan Institute, University of Ljubljana 39,
61111 Ljubljana, Slovenia

Using a wedge type cell, we have studied the S_A–S_C^*, S_C^*–S_C and S_A–S_C phase transition lines in the ferroelectric liquid crystals 4-(2-methylbutyl)phenyl 4′-*n*-octylbiphenyl-4-carboxylate (CE-8) and 2-methylbutyl 4-(4-decyloxybenzylidene)aminocinnamate (DOBAMBC) as a function of cell thickness in the planar geometry. The phase diagram is similar to the one observed using an external magnetic field. A surface induced re-entrant-like phenomenon is also observed. The experimental results are compared with the predictions of a Landau model with surface anchoring and a qualitative agreement was found. The results show that whereas disclination lines are not important for the S_A–S_C^* and S_A–S_C transition lines, these defects have to be taken into account when evaluating the $S_C^* \rightarrow S_C$ transition line. The form of the phase diagram has some important implications for the performance of surface stabilized ferroelectric liquid crystal cells used in electro-optic devices.

1. Introduction

The fascinating thermodynamical, optical and electro-optical properties of ferroelectric liquid crystals in restricted geometries represent an area of growing interest. Motivated by the discovery of fast switching [1] and a high potential for applications [2] in electro-optical devices, much research has been devoted to understanding and controlling the underlying physical mechanisms of surface induced ordering in ferroelectric liquid crystal phases in restricted geometries. The effects of the restricted geometry on the phase transitions S_A–S_C^*, S_A to the unwound S_C and also S_C^*–S_C have been reported previously [3–7], and were supported by the theoretical analysis [8, 9]. In order to clarify the nature of these transitions, we now report theoretical, as well as experimental studies of phase stability and phase transitions for a ferroelectric liquid crystal, constrained in a planar cell with a variable thickness d. In the theoretical section we derive the phase diagram (d, T) of the ferroelectric liquid crystal in the planar geometry. The S_A–S_C^* transition lines will be derived exactly within the Landau theory. The S_C^*–S_C transition line will be evaluated first without taking the formation of disclination lines [10–13] into account. The results, which are believed to be accurate for small anchoring strengths will then be compared with the exact results obtained for infinite anchoring strengths, using the disclination model [10–13]. The experimental part describes the experimental details and the observed phase diagram for a ferroelectric liquid crystal CE-8.

2. Theory

Let us first investigate the effect of a restricted geometry on the S_A–S_C^* and S_A–S_C transitions for the case that these transitions are of second order, and that the helical axis of the S_C^* phase is parallel to the bounding plates. The most interesting aspect of

0267–8292/93 $10·00

this problem is the dependence of the S_A–S_C^* transition temperature on the cell thickness d. It is clear that for thick samples, the S_A phase will transform with decreasing temperature into the helicoidal S_C^* phase, whereas for thin enough samples, this will be replaced by a transition into the homogeneous S_C phase.

The geometry of the problem is illustrated in the inset to figure 1 (*a*). A ferroelectric S_C^* liquid crystal in the bookshelf geometry is confined in a sample cell of thickness $d=2L$. The cell plates are at $x=-L$ and $x=L$, the helical axis is along the z direction and the system is homogeneous along the y direction. The surface anchoring energy will be taken into account in the simple form $\frac{1}{2}C\xi_1^2$, i.e. we shall treat the case of planar non-polar anchoring. Here ξ_1 is out of the plane of projection of the tilt.

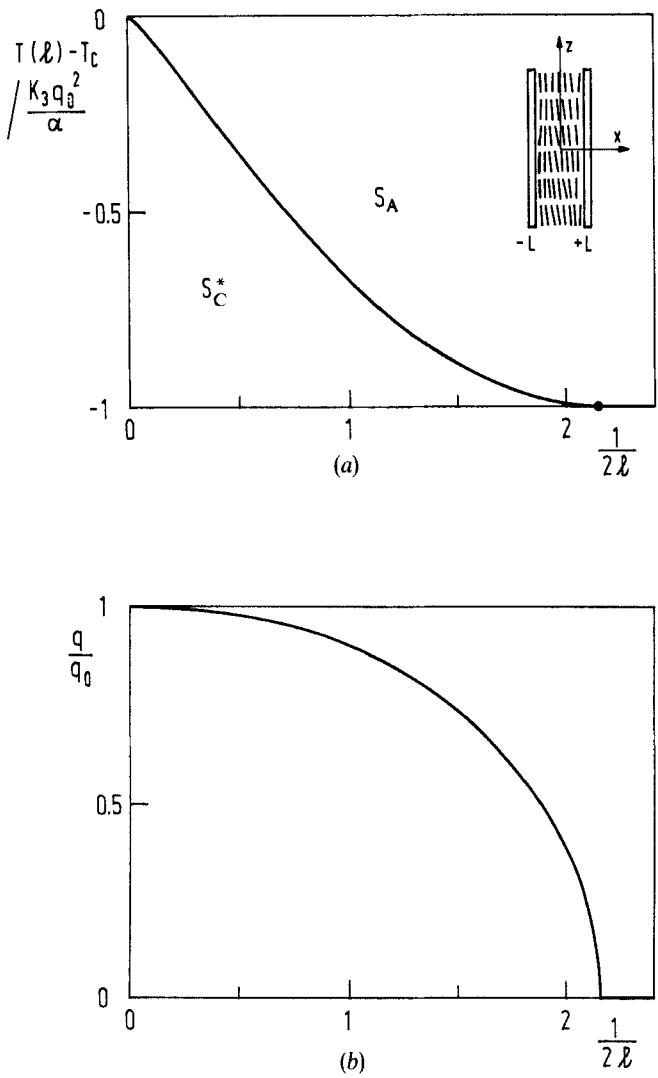

Figure 1. (*a*) dependence of the S_A—S_C^* phase transition line on the inverse of the normalized cell spacing and (*b*) dependence of the wave vector q of the helix along the λ line for $c=0{\cdot}5$. In the inset, the geometry of the problem is shown.

For the stability analysis of the S_A phase, only the harmonic part of the non-equilibrium free energy density g is needed. It can be written in the one elastic constant approximation ($K_{11}=K_{33}=K_3$) as

$$g(x,z)=\tfrac{1}{2}a(\xi_1^2+\xi_2^2)-\Lambda\left(\xi_1\frac{d\xi_2}{dz}-\xi_2\frac{d\xi_1}{dz}\right)+\tfrac{1}{2}K_3\left[\left(\frac{d\xi_1}{dx}\right)^2+\left(\frac{d\xi_2}{dx}\right)^2\right]$$
$$+\tfrac{1}{2}K_3\left[\left(\frac{d\xi_1}{dz}\right)^2+\left(\frac{d\xi_2}{dz}\right)^2\right]+[\delta(x+L)+\delta(x-L)]\tfrac{1}{2}C\xi_1^2. \quad (1)$$

Here $a=\alpha(T-T_0)$. The S_A–S_C^* transition for an unconfined bulk sample is $T_c=T_0+(1/\alpha)K_3q_0^2$, where $q_0=\Lambda/K_3$ is the wave vector of the undeformed helix.

The equilibrium form of the S_C^* order parameter components ξ_1 and ξ_2 is obtained by minimizing the free energy. The corresponding Euler–Lagrange equations for the bulk are

$$a\xi_1-2\Lambda\frac{d\xi_2}{dz}-K_3\frac{d^2\xi_1}{dx^2}-K_3\frac{d^2\xi_1}{dz^2}=0, \quad (2a)$$

$$a\xi_2+2\Lambda\frac{d\xi_1}{dz}-K_3\frac{d^2\xi_2}{dx^2}-K_3\frac{d^2\xi_2}{dz^2}=0, \quad (2b)$$

whereas we have, for the surface part

$$K_3\xi_1'(L)+C\xi_1(L)=0, \qquad \xi_2'(L)=0, \quad (3a)$$

$$-K_3\xi_1'(-L)+C\xi_1(-L)=0, \quad \xi_2'(-L)=0, \quad (3b)$$

where $\xi_1'=\partial\xi_1/\partial x$, etc. We see that the surface energy and the bulk elastic energy compete: the first one seeks to maintain the molecules parallel to the plates of the cell, while the other seeks to maintain the helicoidal variation of ξ_1 and ξ_2 parallel to the z axis. In the z direction we expect periodic sinusoidal solutions of the form

$$\xi_1=f(x)\cos(qz), \quad (4a)$$

$$\xi_2=g(x)\sin(qz). \quad (4b)$$

Inserting (4a) and 4b) into (2a)–(3b) we get the equations for the amplitudes $f(x)$ and $g(x)$

$$af-2\Lambda qg-K_3f''+K_3q^2f=0, \quad (5a)$$

$$ag-2\Lambda qf-K_3g''+K_3q^2g=0, \quad (5b)$$

together with the boundary conditions

$$K_3f'(L)+Cf(L)=0, \qquad g'(L)=0, \quad (5c)$$

$$-K_3f'(L)+Cf(-L)=0, \qquad g'(-L)=0. \quad (5d)$$

We are looking for the stability limit of the S_A phase, $T_c=T_c(L)$ and the periodicity of the corresponding solutions in the z direction: $q=q(L)$. The stability limit will be given by the highest temperature for which a non-zero solution for the director tilt, i.e. for ξ_1 and ξ_2, exists. The periodicity, i.e. the wave vector q, of this solution will show whether the S_A phase transforms into a helicoidal S_C^* ($q\neq0$) or a homogeneous S_C phase ($q=0$).

Since the boundary conditions interfere with the most favourable helicoidal ordering in the S_C^* phase, we expect that for a finite L, the S_A–S_C^* transition will take place at a lower temperature than in the bulk

$$T_c(L) < T_c(L \to \infty).$$

The boundary conditions, on the other hand, do not interfere with a homogeneous tilt in the y direction ($\xi_2 \neq 0$, $\xi_1 = 0$), so that the S_A–S_C transition is expected to occur at $T = T_0$.

We therefore expect that the S_A–S_C^* transition temperature in a restricted geometry will be between the bulk transition temperatures S_A–S_C^* and S_A–S_C

$$T_0 < T_c(L) < T_c(L \to \infty).$$

The above considerations can be put into a quantitative form as follows.

The solutions of the system of differential equations (5 *a* and *b*) will be linear combinations of $e^{\lambda x}$ terms with both real ($\lambda_+ = \lambda$) and imaginary ($\lambda_- = i\mu$) λ values. The solutions will be of the form

$$f(x) = A\cosh(\lambda x) + B\cos(\mu x), \tag{6a}$$

$$g(x) = -A\cosh(\lambda x) + B\cos(\mu x). \tag{6b}$$

Inserting expressions (6 *a* and *b*) into equations (5 *a* and *b*) we get a system of two homogeneous linear equations which has non-trivial solutions for A and B only if the corresponding determinant of the coefficients vanishes. This leads to

$$\lambda^2 = \frac{1}{K_3}[\alpha(T - T_c) + K_3(q + q_0)^2] \tag{7a}$$

and

$$\mu^2 = \frac{1}{K_3}[-\alpha(T - T_c) - K_3(q - q_0)^2]. \tag{7b}$$

The boundary conditions (5 *c* and *d*) lead to an additional system of equations which has a non-trivial solution only if

$$2K_3 + C\left[\frac{1}{\lambda\tanh(\lambda L)} - \frac{1}{\mu\tan(\mu L)}\right] = 0. \tag{8}$$

For a given anchoring strength C, we now look for that value of q which maximizes the transition temperature. Introducing

$$c = \frac{C}{2K_3 q_0}, \qquad t = \frac{\alpha(T - T_c)}{K_3 q_0^2}, \qquad x = q/q_0 \tag{9a}$$

$$q_0 L = l, \qquad \frac{\mu^2}{q_0^2} = \boldsymbol{\mu}^2, \qquad \frac{\lambda^2}{q_0^2} = \boldsymbol{\lambda}^2, \tag{9b}$$

we can put the above set of equations into a dimensionless form

$$1 - c\left\{\frac{1}{(\mu\mathrm{tg})(\mu l)} - \frac{1}{\boldsymbol{\lambda}\tanh(\boldsymbol{\lambda} l)}\right\} = 0, \tag{10a}$$

$$\boldsymbol{\mu}^2 = t - (x - 1)^2, \tag{10b}$$

$$\boldsymbol{\lambda}^2 = t + (x + 1)^2. \tag{10c}$$

We now look for a given c for that value of x_m for which $t=t(x_m)$ is a maximum. The results are presented in figure 1 (*a*) and (*b*) for $c=0{\cdot}5$. We see that the stability limit of the S_A phase $T(L)$ varies from T_c (i.e. $t=0$) for $L\to\infty$ (i.e. $1/2l\to 0$) to T_0 (i.e. $t=-1$) for $1/2l=1/2l_{LP}=2{\cdot}1547$. In the same interval, $x=q/q_0$ changes from 1 to 0. For

$$l>l_{LP}: \quad x_{MAX}\neq 0,$$

whereas for

$$l<l_{LP}: \quad x_{MAX}=0.$$

Hence $1/2l=2{\cdot}1547$ defines, for $c=0{\cdot}5$, the critical point where the S_A–S_C^* and S_A–S_C transition lines join. The variation of wave vector q along the S_A–S_C^* λ transition line can be described by the power law

$$x\propto\left(\frac{1}{2l_{LP}}-\frac{1}{2l}\right)^{0{\cdot}5}. \tag{11 a}$$

The variation of $1+t$ with l can be for $l\to l_{LP}$ similarly described by

$$1+t\propto\left(\frac{1}{2l_{LP}}-\frac{1}{2l}\right)^{2}. \tag{11 b}$$

It can be shown that the above tri-critical point ($t=-1$, $1/2l=1/2l_{LP}$) is in fact a Lifshitz point (LP), where the second order S_A–S_C^*, S_A–S_C and the first order S_C^*–S_C transition lines meet. The phase diagram of a ferroelectric liquid crystal in a planar cell is thus similar to the phase diagram of a ferroelectric liquid crystal with negative diamagnetic anisotropy in an external transverse magnetic field.

The variation of the reduced Lifshitz cell thickness $1/2l_{LP}$ with the reduced anchoring strength c can be obtained analytically by expanding expression (10 *b*) as well as λ^2 and μ^2 in equation (10 *a–c*) around $t=-1$ and $x=0$. One finds

$$l_{LP}=\frac{1}{4}\left\{-\frac{3}{c}+\sqrt{\left[\left(\frac{3}{c}\right)^2+12\right]}\right\}. \tag{12}$$

From the above expression we see that for

$$c\to 0, \qquad \frac{1}{2l_{LP}}\to\infty, \tag{13 a}$$

whereas for

$$c\to\infty, \qquad \frac{1}{2l_{LP}}=\frac{1}{\sqrt{3}}=0{\cdot}5774. \tag{13b}$$

The critical value of the reduced cell thickness thus vanishes when $c\to 0$ and the S_C^* phase is stable for any non-zero cell thickness. For an infinitely large anchoring strength, on the other hand, the critical cell thickness is finite, and by varying the distance between the cell plates, a S_C^*–S_C transition can be induced. The variation of the critical cell thickness l_{LP} with the anchoring strength is illustrated in figure 2.

The S_C^*–S_C unwinding transition can be, for the case of planar anchoring, treated analogously to the cholesteric–nematic transition [14]. For small tilt angles, we can, in the constant amplitude approximation, express the S_C^* order parameters as

$$\xi_1=\theta\sin\phi(x,z), \tag{14 a}$$

$$\xi_2=\theta\cos\phi(x,z). \tag{14 b}$$

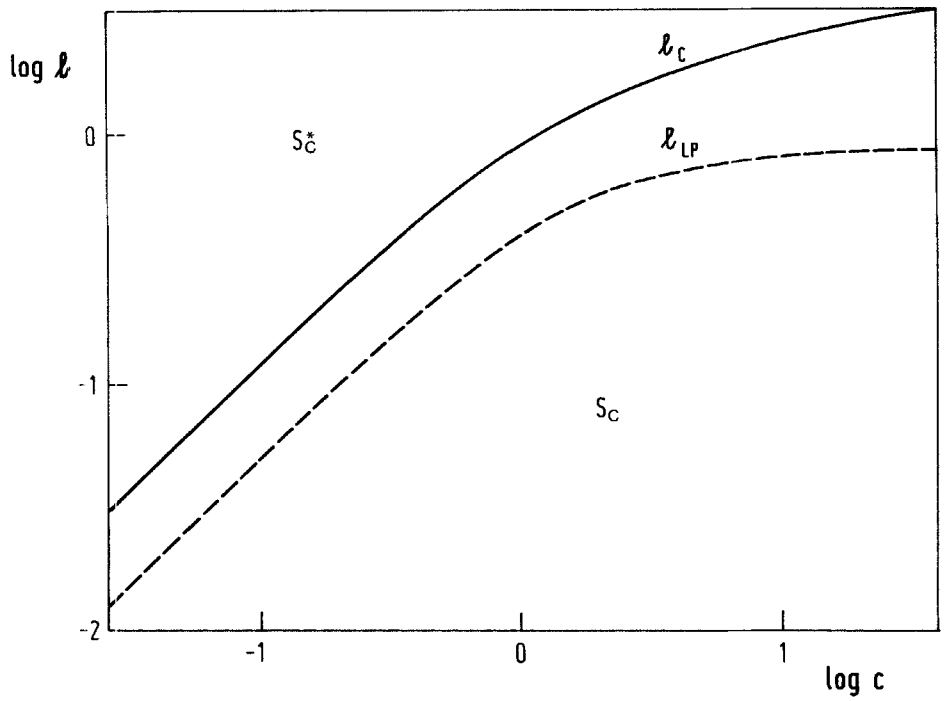

Figure 2. The relation between the critical thicknesses l_C and l_{LP} and the normalized anchoring energy c.

The free energy density $g(x, z)$ for a S_C^* liquid crystal in between parallel plates, see equation (1) can be now written as

$$g(x,z) = -\Lambda\theta^2\frac{\partial\phi}{\partial z} + \tfrac{1}{2}K_{33}\theta^2\left[\left(\frac{d\phi}{dx}\right)^2 + \left(\frac{d\phi}{dz}\right)^2\right] + [\delta(x-L)+\delta(x+L)]\tfrac{1}{2}C\theta^2\sin^2\phi. \quad (15)$$

Dividing the above expression by θ^2, we see that $g(x, z)/\theta^2$ has the same form as the free energy density in the cholesteric case, provided that $\sin^2\phi \approx \phi^2$. By analogy with the cholesteric–nematic transition, we may thus conclude that the free energy will have a minimum for a helicoidal ordering, i.e. a non-zero x

$$x = q/q_0 \neq 0, \qquad l > l_C, \quad (16a)$$

if the plate spacing is larger than a critical value, whereas below a critical plate spacing l_C the minimum free energy will correspond to a homogeneous state, i.e. a zero value of x

$$x = 0, \quad l < l_C. \quad (16b)$$

In the constant amplitude approximation (CAA), which is valid well below the S_A–S_C^* or S_A–S_C λ-line, the transition will be of second order. The critical plate spacing is obtained from the self-consistent equation [14]

$$A(2cl_C) = 2l_C, \quad (17a)$$

where

$$A(k) = \int_0^\infty dx \frac{\tanh x}{x[1 + x/k\tanh x]} = \begin{cases} \tfrac{1}{2}\pi k^{1/2}, & k \leqslant 0{\cdot}1 \\ \ln k + \gamma + \ln(4/\pi), & k > 10 \end{cases} \quad (17b)$$

and $\gamma = 0{\cdot}5772$ stands for Euler's constant. As before $c = C/(2K_{33}q_0)$ and $l = Lq_0$. For $l \to l_C$ the helical pitch diverges logarithmically

$$x = q/q_0 \propto -\frac{1}{l_C}\frac{1}{\ln(l-l_C)}; \qquad 0 \leqslant \frac{l-l_C}{l_C} \ll 1. \tag{18}$$

The variation of the critical cell spacing l_C with the anchoring strength c is shown in figure 2. Whereas the ratio between l_C and l_{LP} is constant for small anchoring strengths c, similarly to the ratio of the so called Lifshitz field and the critical magnetic field in the constant amplitude approximation in the case of a transverse magnetic field, this is not the case for large c values. Whereas l_{LP} approaches a constant for $c \to \infty$, l_C continues to increase with increasing c. The reason for such a behaviour is the fact that there exist only two distinct homogeneous orientations of the director field at the bounding surface in the limit $c \to \infty$. The creation of any domain wall of finite size, that would separate these two domains at the surface, would cost an infinite amount of energy, and is thus energetically unfavourable. As a result of the homogeneous director field at the surface, a homogeneous phase is stable throughout the sample in the CAA, regardless of the sample thickness.

The system can avoid this situation by creating defects, i.e. twist disclination lines [10–13], which allow for the existence of a helicoidal phase between the bounding surfaces even in the limit of infinite anchoring strength. It can be shown [10], that in the limit of infinite anchoring strengths, the critical thickness d_c for the stability of the helicoidal phase is

$$\frac{1}{d_c} = \frac{2\alpha}{p}, \tag{19}$$

where $\alpha = \sqrt{(K_3/K_1)}$ is determined from the elastic constants K_3 and K_1 and $p = 2\pi/q_c$ is the period of the helix in the bulk sample.

The expression for the critical thickness (see equation 17 *a*), as derived within the CAA, is valid in the limit of small anchoring strengths c, and in the absence of twist disclination lines. On the contrary, the stability limit of the S_A phase (see equation (10 *a–c*) is valid for an arbitrary anchoring strength c.

The above form of the phase diagram may have important implications for the production of surface stabilized ferroelectric liquid displays. Such cells are usually produced by filling the cell at higher temperatures and cooling into the S_C phase. If the cell thickness and the anchoring strengths c are such that

$$l_C \geqslant l \geqslant l_{LP}$$

the transition from the S_A to the S_C phase involves the intermediate S_C^* phase, thus creating additional defects. If, however,

$$l \leqslant l_{LP},$$

a direct transition from the S_A to the S_C phase takes place, thus avoiding the above mentioned difficulties.

3. Experimental

The experiment was performed using a wedge-type cell with a maximum thickness of 4·0 μm, controlled by microspacers. The wedge angle was very low, with a typical value of $1{\cdot}5 \times 10^{-3}$. Before filling the cell with liquid crystal material, the local cell spacing was determined from the local interference pattern, as obtained from the

spectrophotometer. The thickness profile thus obtained enabled us to determine the local cell thickness by simply measuring the position of the illuminated spot in the experiment. We were able to determine the local thickness of the cell within 0·1 μm accuracy. In the experiment, we have used optical techniques to determine the phase transition boundaries. The S_A–S_C^* and S_A–S_C transitions were determined from the electroclinic response of the sample, whereas the critical thickness for the surface induced S_C^*–S_C transition was determined from the Bragg diffraction spots, characteristic of the modulated S_C^* phase. In each case, the probing beam was roughly focused, illuminating a 100 μm spot in the sample, so that the measurements are essentially local in the sense that the length of the wedge cell is much larger (typically 15 mm) then the probing area.

When a small, periodic electric field is applied across the planar sample, one obtains in the S_A phase an electro-optical response of the sample due to the coupling of the field to the soft mode. In the S_C^* phase, an additional contribution to the electro-optical response arises, due to the coupling of the phase of the order parameter to the external field. As a result, a change in the direction of the space averaged optical axis of the liquid crystal is induced, which is in the limit of small fields proportional to the probing field. The changes in the direction of the optical axis can be easily detected by an optical technique described elsewhere [15]. It should be stressed that this measuring method is essentially analogous to dielectric response measurements with the advantage of probing the local response of the sample.

In order to determine the thickness dependence of the S_A–S_C^* and S_A–S_C phase transition temperatures correctly, special attention was paid to the temperature gradients in the measuring cell, as well as to the quality of the cells that were used in the experiment. The temperature gradients in the cell were determined by observing the distribution of the clearing point of the liquid-crystalline material. All the data were correspondingly corrected for the observed temperature gradients, resulting in an overall accuracy of $\pm 0{\cdot}1$ K for the temperature.

In the experiment, we have used a PIX-1400 (Hitachi) polyimide alignment layer, deposited by spin coating glass substrates. The alignment layer was left unrubbed, thus representing an isotropic surface with no privileged axis of alignment for the liquid-crystalline molecules. After the cell was filled with liquid crystal material and the temperature gradients were determined, the sample was aligned in a 6·3 T magnet, by slowly cooling (1 K hour^{-1}) from the isotropic phase into the S_A phase. The overall alignment for the CE-8 material, as obtained in a 6·3 T magnet was very good and was significantly better than the alignment in a 2 T magnetic field.

The S_A to the S_C and S_C^* phase transition boundaries were determined from the observed increase in the electroclinic response of the sample when approaching the phase transition point from the S_A phase. The electro-optical responses of the CE-8 cell to a small probing field with frequency $\nu = 1550\,\mathrm{s}^{-1}$, as determined for sample thicknesses 4·1 μm, 3·7 μm, 2·7 μm and 0·95 μm, are shown in figure 3(*a*)–(*d*), respectively. In the case of large thickness (see figure 3(*a*)), one can observe a rather large soft mode contribution to the electro-optical response of the sample near T_c, whereas at lower temperatures, a contribution of the Goldstone mode, which is proportional to q_c^{-2}, is observed. The characteristic peak of the Goldstone mode originates from the maximum in the temperature dependence of the period of the helix in the bulk sample [16]. At smaller thicknesses, but still above the critical thickness, one can observe the shift in the position of the soft mode peak towards the peak of the Goldstone mode. This position of the peak of the Goldstone mode shifts only slightly

(0·1 K) towards lower temperatures at smaller thicknesses. Near the critical thickness, the soft mode peak merges with the Goldstone mode peak, creating a shoulder-like response, as shown in fig. 3 (*c*). Finally, below the critical thickness, the temperature dependence of the electro-optical response is qualitatively different as shown in figure 3 (*d*). From the temperature dependence of the amplitude, we identify [15] the response shown in figure 3 (*d*) as a soft mode, whereas the Goldstone mode response is almost completely suppressed. Some residual response of the phase of the order parameter is still observed below T_c, and we interpret this as originating from the non-uniformity of

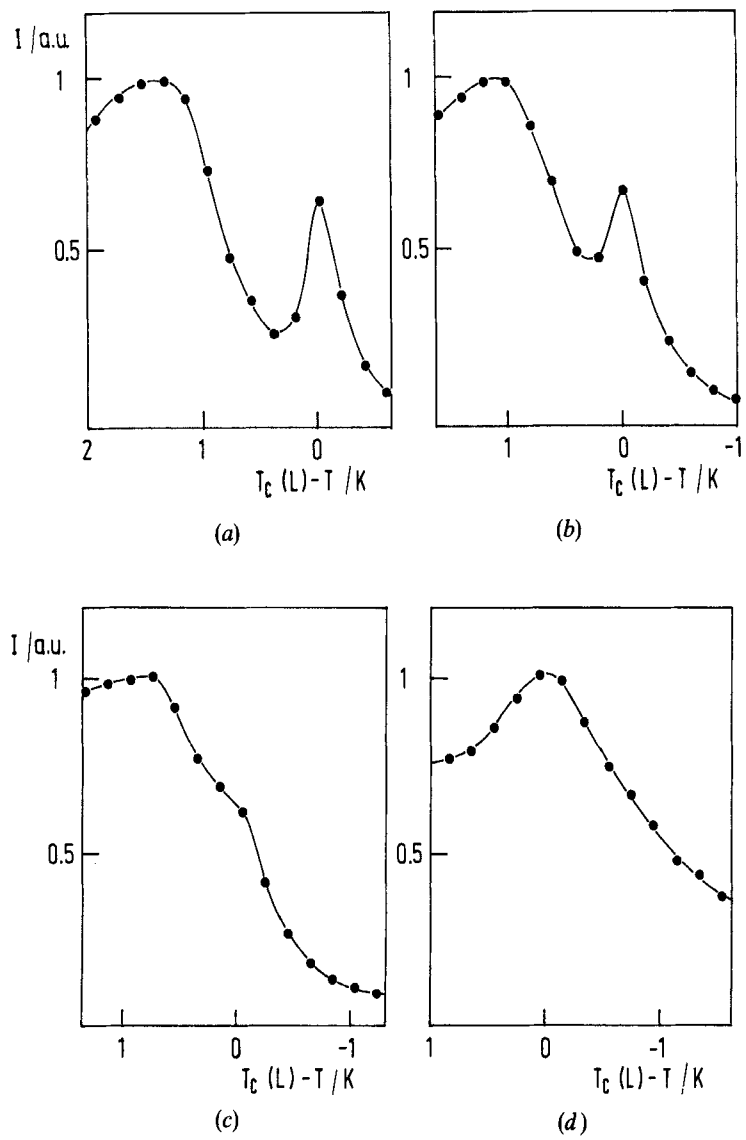

Figure 3. The observed temperature dependence of the electro-optic response of CE-8 at different cell spacings: (*a*) $d = 4{\cdot}1$ μm, (*b*) $d = 3{\cdot}7$ μm, (*c*) $d = 2{\cdot}7$ μm, and (*d*) $d = 0{\cdot}95$ μm. Solid lines are a guide for the eyes only.

the director field within the smectic layers. One should note, that the electro-optical responses of the sample, as shown in figures 3 (*a*)–(*d*) are normalized to the maximum value shown in the figures.

The critical thickness for the surface induced unwinding of the helical structure was determined by observing the local diffraction pattern of the roughly focused He–Ne laser and was defined as the thickness at which the Bragg diffracted peaks disappeared. We were able to determine the critical thickness for CE-8 up to temperatures close to the S_A phase. In a temperature interval 0·3 K near $T_c(L)$, the Bragg scattered light intensity was very low and centred at very high angles, due to the small pitch of CE-8, so that the critical thickness for helix unwinding could not be determined due to experimental limitations.

The surface induced (d, T) phase diagram of 4-(2-methylbutyl)phenyl 4′-*n*-octylbiphenyl-4-carboxylate (CE-8) as observed on PIX-1400 polyimide coated surfaces, is shown in figure 4. One can observe a small (0·5 K) drop in the S_A–S_C^*/S_C transition temperature up to the inverse critical thickness of 0·5 μm^{-1} and then a thickness-independent phase transition line. This is in qualitative agreement with the predicted behaviour of the phase transition temperature along the λ line and beyond the Lifshitz point. It is however impossible at this stage of our experiments to confirm the existence and locate the position of the Lifshitz point in the (d, T) phase diagram. Measurements of q_c along the λ line are thus of crucial importance.

The S_C^* to S_C phase transition line for the surface induced unwinding of CE-8 shows a slight temperature dependence. The critical thickness equals 2 μm at $T_c - T = 5$ K and increases slightly on approaching the S_A phase. This is consistent with the observed temperature dependence of the period of the helix [16] in CE-8, which equals $p_0 = 1{\cdot}2$ μm at $T_c - T = 5$ K and increases slightly on approaching the S_A phase. Very near the S_A phase, a non-monotonous behaviour of the critical thickness as a function of the

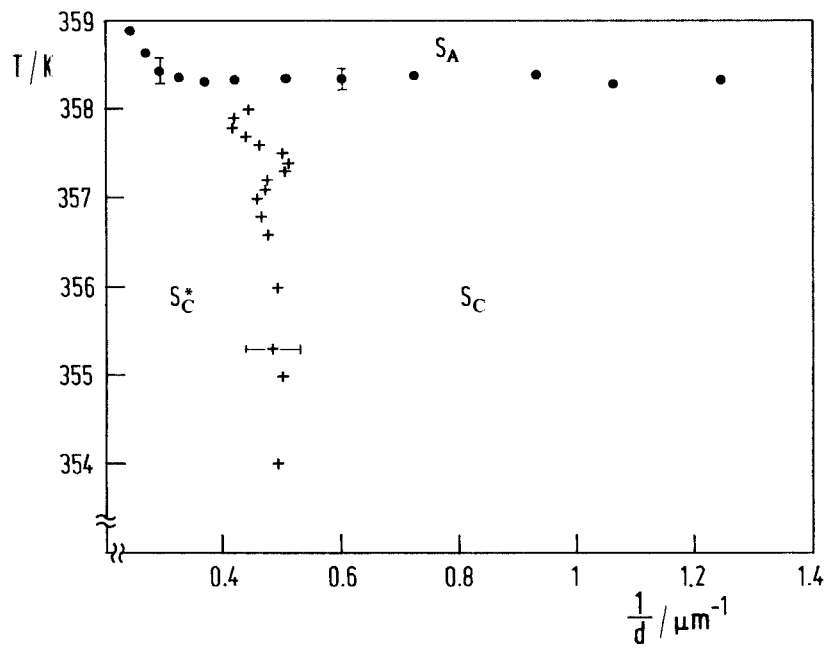

Figure 4. Phase diagram of CE-8 on a PIX-1400 polyimide coated surface.

temperature is observed. A similar behaviour, although on a slightly different temperature scale was observed in the high-resolution measurements of Seppen [17] when determining the Lifshitz point in a (H, T) phase diagram for a mixture of chiral and racemic DOBAMBC. It is not clear what the physical origin of this effect is.

From the normalized critical thickness (see equation (9 *b*)), the period of the helix in bulk CE-8 (1·2 μm), the critical thickness (2 μm) and the magnitude of K_3 (3×10^{-2} N), we obtain an estimate of the normalized critical plate spacing $l_C = 5$. This corresponds, according to figure 2, to $C > 3{*}10^{-3}\,\mathrm{J\,m^{-2}}$. It should be stressed that this large value of the normalized critical thickness l_C indicates that we are in a regime of strong anchoring, which is observed as a saturation of the curve $l_{LP}(c)$ near the value of $\log(c) \approx 0$ in figure 2. This means, that the analysis based on the assumption of a continuous director field is not appropriate, and one has to consider a structure mediated by the appearance of twist disclination lines. As there is no theoretical prediction for the dependence of the critical thickness on the anchoring strength C at intermediate values, we shall compare the predicted critical thickness (see equation (19)) for very strong anchoring to the experimentally observed value. An estimation for α can be obtained from the light scattering data for CE-8 [16, 18] as $\alpha \approx 0{\cdot}3$, resulting in the expected inverse critical thickness $1/d_c \approx 0{\cdot}5\ \mu\mathrm{m}^{-1}$, which is close to the experimentally observed value. This agreement supports the assumption that we are in the regime of very strong anchoring of CE-8 on the polyimide surface and is consistent with the topology of the cells, as observed under the polarizing microscope. Although the pitch of CE-8 is too small to resolve the fine details of the structure under the microscope, one can observe, at large thickness of the sample, an arrangement of lines, resembling the structure, reported for rather large pitch chiral smectics [11]. In the region, where the helix starts unwinding, the density of the observed lines decreases whereas the distance between the lines remains practically unchanged. This is similar to the effect of an electric field on the chiral smectic structure in thin cells [11]. It further supports the existence of disclination lines in thin CE-8 cells, which is characteristic for the case of strong anchoring.

The temperature dependence of the critical thickness in DOBAMBC is similar to the one shown in figure 4 and reflects a slight temperature dependence of the bulk helical pitch in this material. The observed critical thickness for DOBAMBC on the PIX-1400 coated surface is 3·2 μm at $T_c - T = 5$ K, which is close to the value reported previously [6]. This is somewhat larger critical thickness than the one observed for CE-8, but one should keep in mind that DOBAMBC has a larger pitch of 1·7 μm at this temperature.

4. Conclusions

The observed phase diagram of a ferroelectric liquid crystal in a restricted planar geometry is similar to the (H, T) phase diagram of a ferroelectric liquid crystal in a transverse magnetic field and is in qualitative agreement with theory. Whereas the S_A–S_C^* phase boundary shows a slight decrease upon decreasing the cell spacing, the S_A–S_C transition line is spacing independent, within an experimental accuracy of $\pm 0{\cdot}1$ K. The magnitude of the observed temperature drop of the S_A–S_C^* phase boundary with decreasing cell thickness is of the order of magnitude expected from the chiral terms in the free energy expansion. The question about the existence of the Lifshitz point in the (d, T) phase diagram is still open and may be elucidated by the experimental determination of the period of the helical structure along the λ line. Since the experiments indicate that the surface anchoring of CE-8 is rather strong, we can

estimate that the Lifshitz point would appear at $2l_{LP}=\sqrt{3}$ (see equation (13 *b*)), limit $c\to\infty$). Taking $\alpha=0{\cdot}3$, the inverse Lifshitz thickness of the cell is estimated as

$$\frac{1}{d_{LP}}\approx\frac{2\pi}{p}\frac{\alpha}{2l_{LP}}\approx 0{\cdot}91\,\mu\mathrm{m}^{-1},$$

which is twice as small as the critical thickness well below T_c.

References

[1] CLARK, N. A., and LAGERWALL, S. T., 1980, *Appl. Phys. Lett.*, **36,** 899.
[2] CLARK, N. A., and LAGERWALL, S. T., 1984, *Ferroelectrics*, **59,** 25.
[3] PIKIN, S. A., and YOSHINO, K., 1981, *Jap. J. appl. Phys.*, **20,** L557.
[4] KONDO, K., TAKEZOE, H., FUKUDA, A., and KUZE, E., 1982, *Jap. J. appl. Phys.*, **21,** 224.
[5] KONDO, K., TAKEZOE, H., FUKUDA, A., KUZE, E., FLATISCHER, K., and SKARP, K., 1983, *Jap. J. appl. Phys.*, **22,** L294.
[6] KAI, S., NAKAGAWA, M., NARUSHIGE, Y., and IMASAKI, M., 1983, *Jap. J. appl. Phys.*, **22,** L488.
[7] YANG, Y. B., BANG, T., MOCHIZUKI, A., and KOBAYASHI, S., 1991, *Ferroelectrics*, **121,** 113.
[8] YAMASHITA, M., 1983, *J. phys. Soc. Jap.*, **52,** 3735.
[9] YAMASHITA, M., 1984, *Ferroelectrics*, **58,** 149.
[10] GLOGAROVA, M., LEJČEK, L., PAVEL, J., JANOVEC, V., and FOUSEK, J., 1983, *Molec. Crystals. liq. Crystals*, **91,** 305.
[11] GLOGAROVA, M., FOUSEK, J., LEJČEK, L., and PAVEL, J., 1984, *Ferroelectrics*, **58,** 161.
[12] HANDSCHY, M. A., and CLARK, N. A., 1984, *Ferroelectrics*, **59,** 69.
[13] BOURDON, L., SOMMERIA, J., and KLÉMAN, M., 1982, *J. Phys., Paris*, **43,** 77.
[14] LUBEN, M., MUKHAMEL, D., and STRIKHMAN, S., 1974, *Phys. Rev.* A, **10,** 360.
[15] KUCZYNSKI, W., HOFFMANN, J., STRYLA, B., and MALECKI, J., 1990, *Molec. Crystals liq. Crystals*, **192,** 295.
[16] DREVENŠEK, I., MUŠEVIČ, I., and ČOPIČ, M., 1990, *Phys. Rev.* A, **41,** 923.
[17] SEPPEN, A., 1987, Ph.D. Thesis, University of Nijmegen; see also BLINC, R., MUŠEVIČ, I., ZEKŠ, B., and SEPPEN, A., 1991, *Physica scripta*, **T35,** 38.
[18] PINDAK, R., 1991, *Solitons in Liquid Crystals*, edited by L. Lam and J. Prost (Springer-Verlag), Chap. 7.